Engineered Science
DOI: https://dx.doi.org/10.30919/es1398

Parametric Evaluation of Hybrid Hydrogel-Based Colorimetric Assay for Rapid Quantitative Analysis of Uric Acid

Jaturavit Pantakitcharoenkul,[1,*] Kachaporn Mekkhayai,[1,#] Kancharos Paengkhumpung,[1,#] Alireza Asgharpour,[2] Matthew Coblyn,[2] Warangkana Pornputtapitak,[3] Goran Jovanovic[2] and Kulachart Jangpatarapongsa[1]

Abstract

Colorimetric assays offer a fast and accurate quantification of uric acid in biological samples. However, commercial kits require multiple preparation steps and are prone to user errors. In this work, a hydrogel-based uric acid colorimetric assay is developed in conjunction with computational modeling to study the key parameters that govern assay performance and rapidity. Hybrid alginate/polyvinyl alcohol (PVA) hydrogels demonstrate superior shape retention compared to single-type hydrogels. The developed assay shows a linear range of 2-600 µM with a detection limit of 1.92 uM. The computational model provides a good prediction of the dynamic readout profile of fluorescent intensity. The enzyme in hydrogel-based assays shows a prolonged stability compared to a paper-based immobilization approach, maintaining the effectiveness after 4 months of storage under the same conditions. The fastest result from the hydrogel-based assay was achieved within 15 minutes. The circumscribed central composite design, implemented with the computational model, revealed the significance of enzyme concentration and uric acid diffusivity in the hydrogel on the readout time. The quadratic model demonstrated strong predictive potential, suggesting its possible application for further development of hydrogel-based assays.

Keywords: Hydrogel; Uric acid; Biosensor; Enzymes; Rapid assay; Hyperuricemia.
Received: 30 October 2024; Revised: 06 January 2025; Accepted: 07 January 2025.
Article type: Research article.

1. Introduction

Hyperuricemia is a prevalent disease that requires early screening and treatment to prevent progression to more severe disorders. Excessive plasma urate concentration (more than 7 mg/dL) can develop into other rheumatic conditions, including gouty arthritis,[1,2] and potentially lead to renal failure in patients with metabolic syndrome.[3] Patients with renal impairments, such as end-stage renal disease (ESRD), acute kidney injury (AKI),[4] or chronic kidney disease (CKD),[5,6] are at risk of developing hyperuricemia, except for those with chronic or acute gouty arthritis.[7] Hyperuricemia can be classified as symptomatic or asymptomatic. Asymptomatic patients are often unaware of the disorder due to the absence of signs of urate crystal deposition. This condition is concerning because prolonged elevation of plasma uric acid can increase the risk of tissue damage and cardiovascular disease.[8] The disease is diagnosed in more than 10% of the Thai population,[9] directly affecting individuals' quality of life. The modern practice of uric acid testing requires medical personnel to collect blood or urine samples, with specific analysis techniques performed only by medical technicians.[10] As a result, preventing and mitigating the disease cannot occur without clinical assessment. Although urine and blood strip tests are available for self-screening, they remain unaffordable. In conclusion, Southeast Asian countries need a more cost-efficient and faster approach to preliminary hyperuricemia screening.

In-vitro diagnostic devices have been developed to serve as rapid testing methods. In recent years, paper-based and

[1] *Center for Research Innovation and Biomedical Informatics, Faculty of Medical Technology, Mahidol University, Nakhon Pathom, 73170, Thailand*
[2] *School of Chemical, Biological, and Environmental Engineering, College of Engineering, Oregon State University, Corvallis, 97333, USA*
[3] *Department of Chemical Engineering, Faculty of Chemical Engineering, Mahidol University, Nakhon Pathom, 73170, Thailand*
[#] *These authors contributed to this work equally.*
**Email:* Jaturavit.pan@mahidol.edu (J. Pantakitcharoenkul)

electrochemical sensors have shown promising results in detecting uric acid in serum and urine.[11] One such device is the lateral flow assay (LFA), an in-vitro diagnostic tool that effectively identifies various analytes, such as antigens and antibodies. Owing to its cost-effectiveness and simplicity of assembly, LFAs can serve to identify a wide range of diseases,[12] most notably in COVID-19 rapid tests. This detection method has seen rapid development through the integration of advanced materials. A computational model facilitates time-scale analysis of essential components in LFA and rapid detection assays. The simulation of transport phenomena helps optimize various aspects of detection, including flow distribution, diffusion of reactants, reaction rate, and assay geometry.[13]

In addition to nanoparticle-conjugated antibodies in LFA, enzymes have been extensively studied for their applications as labels in lateral flow immunoassay. Urate oxidase, or uricase, reacts specifically with uric acid to convert it into a water-soluble compound, 5-hydroxyurea, and quantifiable hydrogen peroxide in a one-to-one reaction. Because of this advantage, the enzyme has been utilized for both hyperuricemia treatment and uric acid detection. Various platforms, such as nanostructured carriers,[14] enzymosomes,[15] and hydrogels,[16,17] have been investigated to accommodate urate oxidase for uric acid analysis. The use of protein immobilization techniques, such as physical entrapment or covalent binding, enables many therapeutic and diagnostic approaches, such as in-vivo delivery of uricase,[16] circulation half-life prolongation,[18] and biosensor development.[19,20] Hydrogels exist in a wide range of polymer choices and are known for their biocompatibility,[17] cost-effectiveness, and protein entrapment efficiency. Sodium alginate (SA) and poly (vinyl alcohol) (PVA) are among the current options. Due to their ease of fabrication and low cost, both hydrogels are common choices for medical applications and enzyme immobilization, often in the form of beads or bio-printed hydrogel.[21] The blended formulation of different polymer types has also shown improved mechanical properties and sensitivity in biosensors.[22,23] As a thin film layer, these functionalized hydrogels can be integrated within microfluidic or microscale-based architectures, enabling the development of medical devices such as electrical biosensors or extracorporeal treatment units. Hydrogel in medical devices should possess suitable physical and chemical characteristics according to the intended applications. The most ideal hydrogel features for enzyme immobilization include hydrophobicity, biocompatibility, high porosity, and large pore area to maximize catalytic reaction capacity.

Hydrogel-based assays can serve as an alternative to LFA for enzymatic in-vitro diagnostics. The development of uricase-functionalized assays is a common approach for faster quantification of serum uric acid. Although most recent enzymatic sensors offer physical and detection improvements, the designs remain complicated and require several preparation steps.[24] Additionally, challenges such as lifespan, storage, and fluctuating enzyme stability make them impractical for commercialization.[25] Hydrogel entrapment is one strategy for prolonging enzymatic activity by providing a more natural milieu to prevent protein deformation from external exposures.[26]

This study proposes a simple yet effective innovation for uric acid quantification that addresses several shortcomings of commercial assay kits using a rapid detection method. The colorimetric method incorporates two reaction steps: first, the degradation of urate into hydrogen peroxide and allantoin, catalyzed by urate oxidase; second, the activation of resorufin through the conversion of Amplex Red (10-acetyl-3,7-dihydroxyphenoxazine) by hydrogen peroxide in the presence of horseradish peroxidase (HRP) (Fig. 1). The concurrent development of a computational model will assist in optimizing device design and parametric studies. The simulation also provides a method of investigation that could influence the development of next-generation devices for detecting other uremic toxins or analytes.

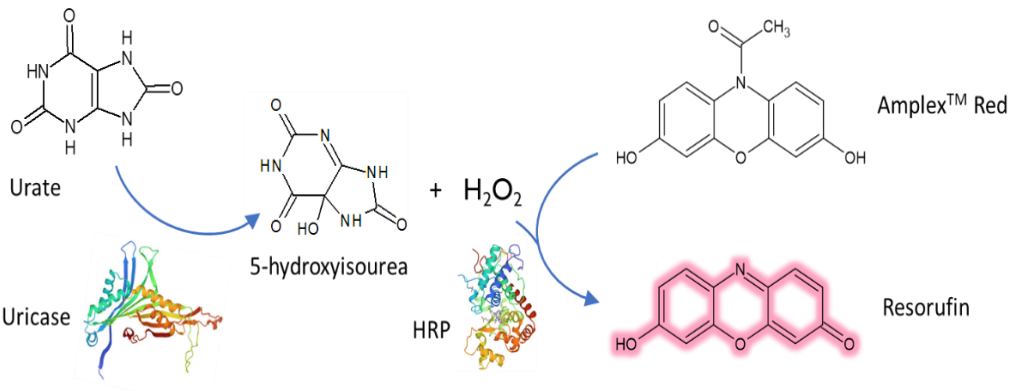

Fig. 1: Reaction schematic of the enzymatic hydrogel-based uric acid rapid assay.

2. Experimental section

2.1 Chemicals

Lyophilized uricase, horseradish peroxidase, Amplex Red, dimethylsulfoxide (DMSO), uric acid, hydrogen peroxide, and 0.5 M Tris-HCl were purchased from Thermo Fisher Scientific, USA. PVA powder (MW 89,000 – 98,000, 99% hydrolyzed) and calcium chloride were purchased from Sigma-Aldrich, USA. Alginic Acid Sodium Salt (AASS) was purchased from Glentham Life Sciences, United Kingdom.

Table 1: Hydrogel formulations used in this study.

Samples	AASS content (%W/W)	PVA content (%W/W)	Gelling temperature
SA2	2	-	Room temp.
SA3	3	-	Room temp.
PVA10	-	10	-20 to 4 ºC
PVA15	-	15	-20 to 4 ºC
HB110	0.5	5	-20 to 4 ºC
HB210	1	5	-20 to 4 ºC
HB310	1.5	5	-20 to 4 ºC

2.2 Hydrogel-based assay preparation

Enzyme solutions were prepared by reconstituting lyophilized horseradish peroxidase (HRP) in 0.1 M Tris-HCl buffer at pH 7.5 and lyophilized uricase in deionized water, with final enzyme concentrations of 100 U/mL each. The working solution was prepared by dissolving 0.26 mg of Amplex Red reagent in 100 µL of DMSO, followed by mixing this solution with the enzyme solutions in a 5:2:2 HRP: Uricase: Amplex Red volume ratio.

Three types of hydrogels, including calcium alginate, PVA, and hybrid Calcium alginate-PVA, were prepared following the formulations listed in Table 1. For alginate hydrogels, alginic acid sodium salt powder (Thermo Fisher Scientific, USA) was gradually poured into heated deionized water and stirred at 200 RPM to prevent clump formation. The clear gel solution was sonicated and left overnight at 4 °C before gelling. Alginate solutions were conditioned to room temperature and dialyzed for 6 hours before being mixed with the working solution at a final enzyme concentration of 0.4 U/ml. The prepared solution was crosslinked by spraying with a 27 mM calcium chloride solution. The gelled calcium alginate hydrogels were stored in the refrigerator overnight to equilibrate. For PVA, the polymer powder was stirred in deionized water at room temperature, then gradually heated to 60 °C until dissolved. The prepared solution was sonicated to ensure uniform porosity and prevent any polymerization from cold temperatures. The PVA gel solution was mixed with the working solution to the same final enzyme concentration of 0.4 U/ml and vortexed to ensure uniformity. The samples were treated with 6 freeze-thaw cycles, ranging from -20 (16 hours) to 4 °C (8 hours). Prepared hydrogels were washed with pH 7.0 Tris-HCl buffer 5 times to rinse off surface-adsorbed enzymes and unreacted crosslinker. For hybrid hydrogel samples, prepared alginate and PVA solutions were mixed in a 1:1 ratio according to their respective formulations. For example, 100 g of HB310 is prepared by mixing 50 g of SA3 with 50 g of PVA10. The prepared solutions were homogenized and sonicated to ensure homogeneity, then left overnight to degas. Hybrid hydrogels were crosslinked by freeze-thawing for 6 cycles under the same conditions as the PVA samples.

2.3 Swelling degree and apparent characteristics

Hydrogels were measured for their original weights (W_0) post-synthesis and freeze-dried for 24 hours (Scanvac CoolSafe Pro) before further measurement. Infrared spectra were collected using attenuated total reflection Fourier-transform infrared spectroscopy (ATR-FTIR, Thermo Fisher Scientific, USA) in the range of 3600 to 650 cm-1 to confirm polymer crosslinking and the uniformity of enzyme entrapment. Cross-sectional morphologies were studied via scanning electron microscopy (SEM, JEOL JSM-IT500LA, Japan). BET analysis was performed to examine the sample's porosity features.

Freeze-dried samples were measured for their dry weights (W_D) before being submerged in deionized water. Samples were weighed (W_s) at 5, 10, 15, 30, 60, 120, 240, and 360 minutes. The swelling ratio and moisture content were calculated with Eq. (1).

$$Swelling\ ratio = \frac{W_s - W_D}{W_D} \quad (1)$$

where W_s is the swollen weight of the hydrogel at a specific time point, and W_D is the dry weight of the sample. All samples were measured in triplicate from separated preparations.

2.4 Colorimetric uric acid measurement and stability assessment

Prepared hydrogel assays were stored at room temperature and 4 °C to determine the enzyme stability and shelf-life over different storage periods. Samples were tested for their ability to detect uric acid after storage at post-synthesis and at 7, 30, 60, and 120 days. A fluorescent spectrophotometer was employed to measure hydrogen peroxide generation from the catalysis within the detection range of 573 – 608 nm. Enzymatic hydrogel assays were tested for their efficacy in detecting uric acid. Uric acid samples were prepared by mixing lyophilized uric acid with deionized water to obtain sequential concentrations of 600, 300, 150, 75, 37.5, 15.625, 7.813 and 0 µM. A 10 µL aliquot of each solution was

transferred to sample and control wells containing functionalized hydrogel. Concentration profiles and readout time were utilized as objective functions for computational model optimization.

2.5 Hydrogel-based assay computational model development

A computational model will be developed in COMSOL Multiphysics version 6.0 to investigate the mass transport and enzymatic reactions in a time-dependent study. The 2-dimensional axisymmetric geometry of the hydrogel well was set up as illustrated in Fig. 2 to represent the 3-dimensional geometry of a hydrogel. Darcy's law was used to determine fluid flow in the hydrogel matrix. For this model, the following assumptions are made:

1. In the hydrogel, enzymes and Amplex Red are immobilized homogenously at known concentrations.
2. Mass transport occurs in the z and r directions.
3. There is no mass flux of species at the edge or the bottom of the hydrogel. The boundary conditions are in Eqs. (2) and (3).

$$z = 0,\ \frac{\partial C_i}{\partial z} = 0 \tag{2}$$

$$r = R,\ \frac{\partial C_i}{\partial r} = 0 \tag{3}$$

4. Species transport follows the equation of continuity expressed in terms of molar flux in cylindrical coordinates.
5. Mass transport occurs only through diffusion only (v = 0).

In the hydrogel well, uric acid concentration follows the equation of continuity, expressed in terms of molar flux (j_i) in cylindrical coordinates using Eq. (4).

$$\left(\frac{\partial C_i}{dt} + v_r\frac{\partial C_i}{\partial r} + \frac{v_\theta}{r}\frac{\partial C_i}{\partial \theta} + v_z\frac{\partial C_i}{\partial z}\right) = -\left[\frac{1}{r}\frac{\partial}{\partial r}\left(rJ_{i,r}\right) + \frac{1}{r}\frac{\partial J_{i,\theta}}{\partial \theta} + \frac{\partial J_{i,z}}{\partial z}\right] + \Delta r \tag{4}$$

For the first boundary condition, the Gaussian pulse function is used to simulate sample dropping and introduction of the uric acid using general inward flux (J_{UA}), expressed in Eq. (5) as:

when $z = h,\ t = 0$,

$$J_{UA}(t) = \frac{\int_0^{t_{drop}}\left(\alpha^{\left(-\frac{(t-b)^2}{2\sigma^2}\right)}\right)dt \cdot C_{UA,sample}V_{sample}}{\pi {r_{droplet}}^2} \tag{5}$$

where t_{drop} is the time taken for a droplet to fully adsorb into the hydrogel layer (0.3 s), $\alpha = \frac{1}{\sigma\sqrt{2\pi}}$, b is the value of the peak in the Gaussian function, and σ is the standard deviation of the Gaussian function, with an integration value of 1.

As stated in the assumptions, mass transport occurs only through diffusion in the r and z directions. Thus, Eq. (4) can be rewritten as Eq. (6):

$$\left(\frac{\partial C_i}{\partial t}\right) = -\left[\frac{1}{r}\frac{\partial}{\partial r}\left(rJ_{i,r}\right) + \frac{J_{i,z}}{\partial z}\right] + \Delta r_i \tag{6}$$

Fick's law describes molar flux due to diffusion in the x direction ($J_{i,x}$), given by:

$$J_{i,x} = -D\frac{\partial C_i}{\partial x} \tag{7}$$

By applying the assumptions and substituting Eq. (7) into Eq. (6), the mass transport model can be rewritten as Eq. (8):

$$\frac{\partial C_i}{dt} = D\left[\frac{1}{r}\frac{\partial}{\partial r}\left(r\frac{\partial C_i}{\partial r}\right) + \frac{\partial^2 C_i}{\partial z^2}\right] + \Delta r_i \tag{8}$$

where Δr_i denotes the net rate change of species i in the hydrogel layer. In Eqs. (5) and (7), the conversion rate of uric acid to hydrogen peroxide is governed by Michaelis-Menten kinetics, whereas the conversion of hydrogen peroxide to resorufin is assumed to follow pseudo-first-order kinetics with the rate constant (k''), as HRP is present in excess compared to hydrogen peroxide generated. Hence, the net rates of each species can be written as follows, seen Eqs. (9)-(11):

$$\Delta r_{UA} = -\frac{v_{max,uox}\cdot C_{UA}}{K_{M,uox}+C_{UA}} \tag{9}$$

$$\Delta r_{H_2O_2} = \frac{v_{max,uox}\cdot C_{UA}}{K_{M,uox}+C_{UA}} - k''C_{H_2O_2} \tag{10}$$

$$\Delta r_{Res} = k''C_{H_2O_2} \tag{11}$$

3. Results and discussion

3.1 Hydrogels characteristics

Hydrogel films were prepared with different formulations to evaluate their apparent and physical characteristics. Post-preparation, the gels were freeze-dried for 48 h before further investigation, with apparent shrinkage shown in Fig. 3. Pure alginate and PVA hydrogels (SA3 and PVA10) showed visible

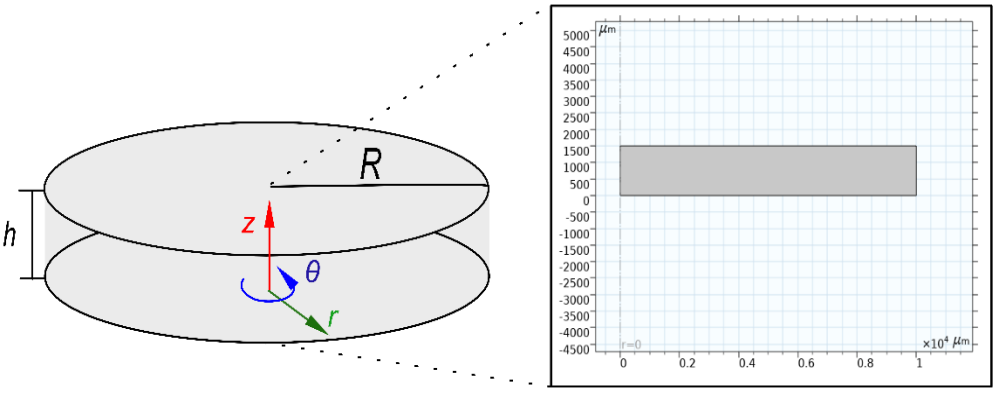

Fig. 2: The axisymmetric schematic of a hydrogel model representing the 3-dimensional cylindrical hydrogel geometry.

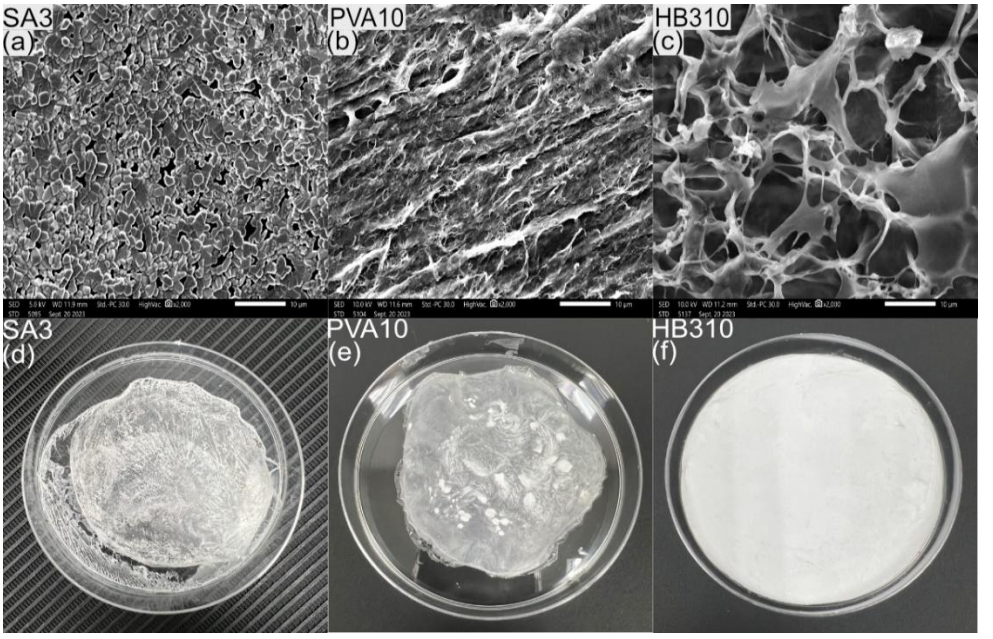

Fig. 3: Appearance of freeze-dried hydrogel films (a) SA3, (b) PVA10, and (c) HB310 and their corresponding microscopic structures obtained from SEM (d) SA3, (e) PVA10, and (f) HB310. The scale bar represents 10 µm.

shrinkage in post-drying diameters. Hybrid hydrogels (HB310) revealed minimal shrinkage in gel diameter, likely due to reduced hydrogen bond formation caused by alginate interference during the freeze-thawing process. SEM images suggest surface crystallinity in calcium alginate samples (SA2 and SA3), formed by calcium ions and carboxylic groups, whereas PVA hydrogels (PVA10 and PVA15) show more closely packed gel fibers with few visible pores. Interestingly, the hybrid polymer sample (HB310) exhibits mixed properties observed in both PVA and alginate hydrogels. The surface morphology suggests an enlarged pore size, which could improve the uniformity of liquid distribution in the gel matrix. Hydrogel solutions were prepared according to the previously described formulations in Table 1. Each formulation was quantified for its porous properties using BET analysis, with the results depicted in Table 2. Notably, distinct porous surface area values were found in the hybrid samples, specifically HB110 and HB210. The former had the highest surface area at 24.460 m^2/g, supporting the homogeneity of the reaction, while the latter had the largest pore volume at 0.189 cc/g, which could enhance diffusivity and reaction velocity in the assay.

Although every hydrogel sample exhibited the same rate of water uptake, dynamic swelling profiles shown in Fig. 4 indicate the highest absorbed volume in calcium alginate hydrogels (SA2 and SA3), likely due to the water-absorptive nature of the polysaccharide backbone in alginate. Pure PVA hydrogels, although having the same rate of water uptake as alginate hydrogels, showed the lowest uptake volume due to the hydrophobic hydrocarbon backbone. Interestingly, the dynamic swelling of hybrid hydrogels (HB110, HB210, and HB310) shows a competitive swelling rate with a plateau between the PVA and SA samples at swelling degrees of 10 – 15. The increase in alginate content caused a slight upward shift in the degree, owing to the high water-retention capacity of the carbohydrate backbone.

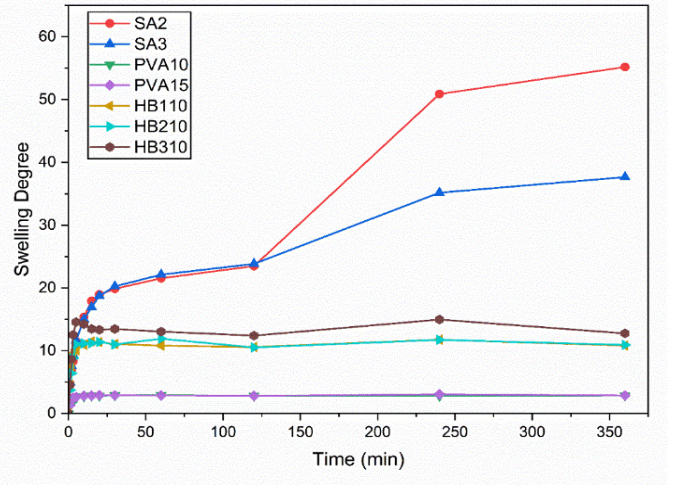

Fig. 4: Dynamic swelling degree of the hydrogel samples.

The DSC spectrum shown in Fig. 5(a) depicts the glass transition phase in all samples at the start of the test (0 °C), which is expected for hydrogel films. PVA10 exhibited a crystallization temperature of 225 °C, whereas SA3 and HB310 showed identical early onset temperatures of 25 °C. Interestingly, a crystallization temperature peak was observed for HB310 at 225 °C, likely due to the PVA portion of the sample. SA3, on the other hand, showed possible decomposition at temperatures above 200 °C.

In Fig 5(b), the FT-IR spectra suggest visible changes in the chemical composition of the hybrid sample (HB310). Pure alginate hydrogel (SA3) shows strong COO- peaks at 1410 cm^{-1} and 1600 cm^{-1}. Pure PVA hydrogel (PVA10) exhibits CH-

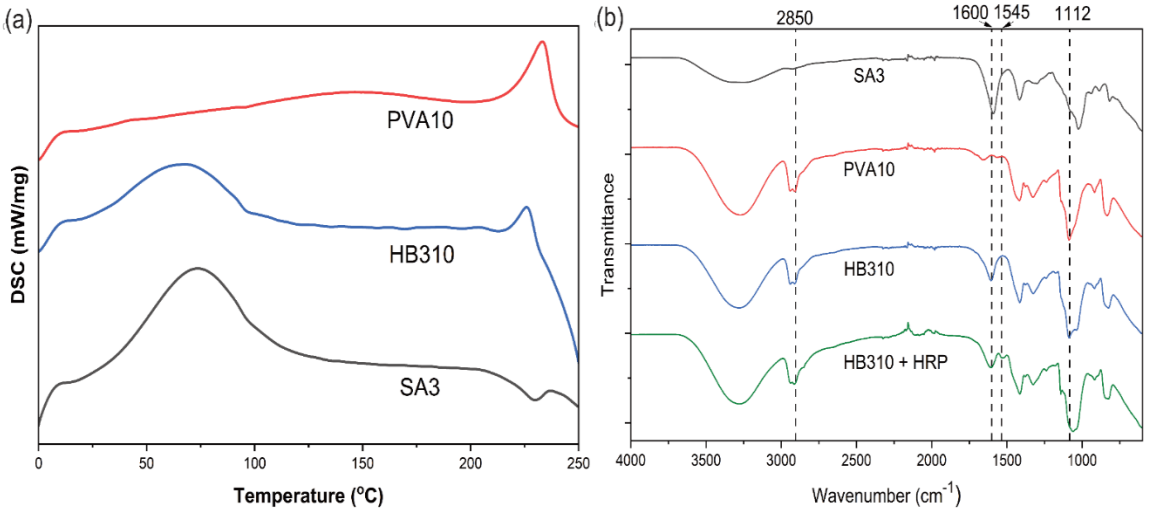

Fig. 5: (a) DSC spectra of PVA10, HB310, and SA3 hydrogel films and (b) FTIR spectra of PVA10, SA3, HB310, and HB310 with horseradish peroxidase hydrogel films.

Table 2: Comparison of colorimetric uric acid detection methods and this work.

Detection method	Linear range (µM)	Limit of detection (µM)	Sample volume (µL)	Reference
Uricase/MIL-53(Fe)	4.5-60	1.30	100	[27]
TMB-Chitosan-Au NPs/uricase	0.1-30	0.04	50	[28]
IL-capped NiNPs	0.01 – 2.40	0.13	100	[29]
MoS_2-catalyzed TMB-H_2O_2	0.5 - 100	0.3	50	[30]
Carbon quantum dots co-doped with iron and nitrogen (Fe@NCDs)	2-150	0.64	200	[31]
PVA-SA/Uricase-HRP-AR	2 – 600	1.92	10	This work

stretching observed from the peaks at 2850 and 2750 cm^{-1}, along with the broad and strong -OH group from the PVA chain expressed at wavelengths of 3000 – 3500 cm^{-1}. Interestingly, both distinct chemical characteristics from SA3 and PVA10 are present in HB310. The reduction in intensity of the -OH group supports the interference of alginate in hydrogen bond formation between hydroxyl groups. Higher expression of alginate can be observed from the increased peak intensity at 1600 cm^{-1}. After immobilization of horseradish peroxidase, noticeable shifts in peaks, especially at 1545 cm^{-1}, representing the amine groups on the enzyme's surface.[25] Peaks at 1112 cm^{-1}, representing aliphatic amines (C-N stretching), were observed, indicating high immobilization efficiency in all samples.

3.2 Performance evaluation of the hydrogel-based assays

Quantitatively, all samples exhibited the good signal linearity (R^2 > 0.90) after 20 min of sample incubation with varying uric acid concentrations, as shown in Fig. 6. Hybrid hydrogel samples and PVA10 yielded relatively high R^2 values, showing potential for use as a colorimetric assay. For assay and model validation, HB310 was chosen based on its linearity and shape retention characteristics. A prototypic hydrogel-based assay was created using a 3D-printed mold containing a 3.5 mm radius pocket with a 0.5 mm thickness to accommodate the hydrogel layers. Fig. 7 shows the apparent visual quality of the colorimetric hydrogel-based assay prepared with HB310 after exposure to uric acid solution samples at concentrations of 600, 300, 150, 75, 37.5, 18.75, and 0 µM. Vivid, distinctive color intensities corresponding to increasing concentrations can be observed with the naked eye. Limit of detection (LOD) analysis was performed to determine the lowest concentration of uric acid that can be measured using the hydrogel-based assay. The LOD was determined to be 1.92 µM, based on the calculated standard deviation of the blank samples and the slope of the calibration curve. Compared to other studies with similar uric acid quantification methods (Table 2).[27-31] The hydrogel-based assay demonstrated competitive detection

performance with a versatile linear range of 2–600 µM, making it suitable for hyperuricemia screening using only 10 µL of sample and requiring no pretreatment.

Hydrogel-based assays with identical enzyme concentrations (0.4 U/mL of uricase and 0.4 U/mL of HRP) were analyzed for their readout times. Fig. 8(a) illustrates the normalized relative fluorescent unit over time after introducing 10 µL of 600 µM uric acid solution. HB210 and PVA10 demonstrated the shortest final readout time at 15 min. This could be correlated with the previously discussed porous properties of the hybrid polymer samples. Although this is not evident in the PVA samples, where PVA15 has higher values in both surface area and pore volume, the final readout time is much slower compared to PVA10. This may be due to the increased inhibition of the enzymatic reaction as the polymer content increases. This phenomenon is more apparent in alginate samples (SA2 and SA3), as the hydrogel matrix can obstruct both mass transport and the reactions of uric acid and hydrogen peroxide.[32]

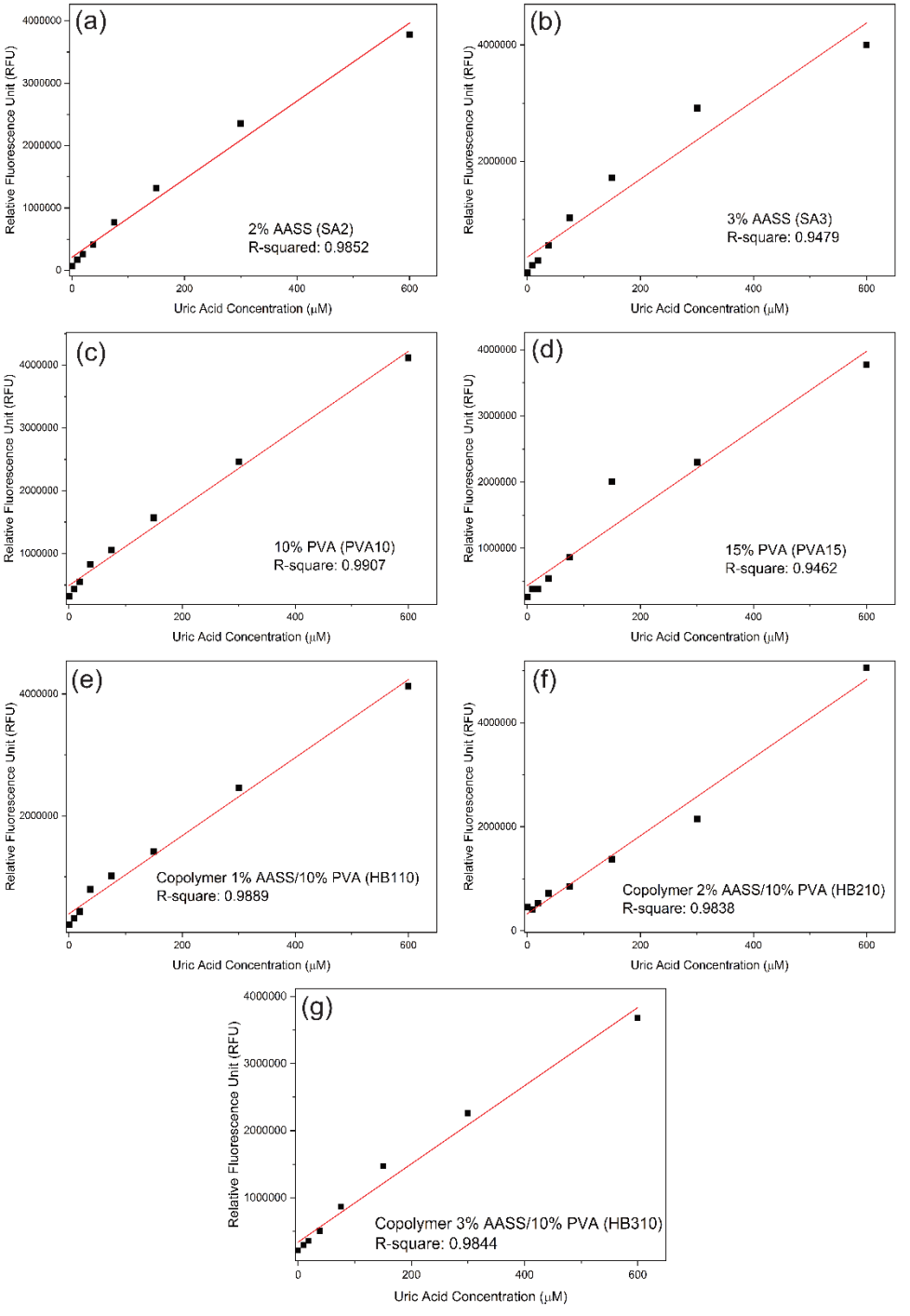

Fig. 6: Linearity of quantitative analysis of uric acid concentration from hydrogel-based assays (a) SA2, (b) SA3, (c) PVA10, (d) PVA15, (e) HB110, (f) HB210, and (g) HB310. All formulations demonstrated substantial linearity ($R2 \geq 0.98$) within the uric acid concentration range of 2 – 600 µM.

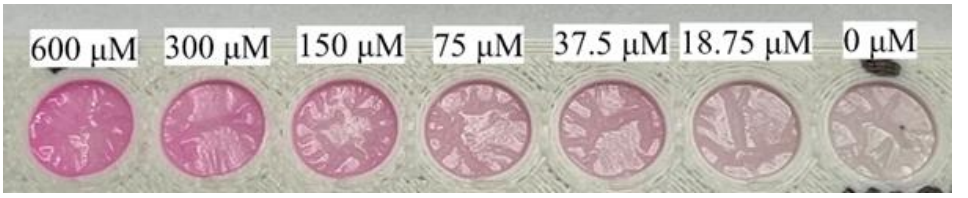

Fig. 7: Visual quality of the readout from hydrogel-based uric acid assay.

The developed mathematical model was validated with the normalized concentration profile of resorufin, measured through fluorescence intensity. Relevant kinetic parameters, including the Michaelis constant ($K_{M,uox}$) and maximum velocity ($v_{max,uox}$) of uricase at a concentration of 0.4 U/mL, were determined using a Lineweaver-Burke plot generated through a separated experiment, yielding values of 0.186 mM and 0.883 mM/min, respectively. The mathematical model was fitted with the signal readout data from HB110, due to its highest linearity among the hybrid samples. The developed model showed an excellent fit with the concentration profile of the hydrogel sample, with R^2 = 0.99 (Fig. 8(b)). The parameter estimation revealed the diffusivity value of HB110 to be 6.372 × 10^{-12} m/s. Both the experiment and simulation yielded a final readout time of 15 min after sample introduction. The strong alignment between the two profiles suggests the potential use of the mathematical model for parametric evaluation of hydrogel-based assay.

3.3 Immobilized enzyme stability testing

The stability of the HB310 hydrogel-based assay was evaluated by comparing signal intensity after defined storage periods at 4 °C to that of the paper-based immobilization approach. Fig. 9(a) depicts the apparent signal readout for both assays before and after sample introduction. Notably, the functionalized Whatman paper in the paper-based assay exhibited a pale pinkish color even before sample introduction, while the hydrogel-based assay maintained its original hue after storage. This observation suggests potentially lower enzyme stability within the paper matrix compared to the HB310 hydrogel. After the introduction of uric acid, HB310 hydrogel produced a more vivid fluorescent color of resorufin than the paper-based assay, even after 1-month of storage. Fig. 9(b) shows the measured signal intensity of hydrogel and paper-based assays at post-synthesis and after 7, 30, 60, and 120 days at 4 °C. Although both assay configurations showed decreased signal intensity after storage, the readout signal from the hydrogel samples remained higher, with a 53.63 % reduction in fluorescent intensity compared to the 68.29% reduction observed in the paper-based assay after 4 months. These findings suggest a prolonged shelf life for the hydrogel-based assay compared to paper-based immobilization or conventional assay kits under the same storage conditions.

3.4 Mathematical model validation and parametric study of hydrogel-based

The design of the experiment was implemented using the developed computational model to perform a parametric study. Three parameters including hydrogel thickness, uricase concentration, and substrate diffusivity in the gel matrix were studied for their effects on signal readout time. Acircumscribed central composite design was utilized with a

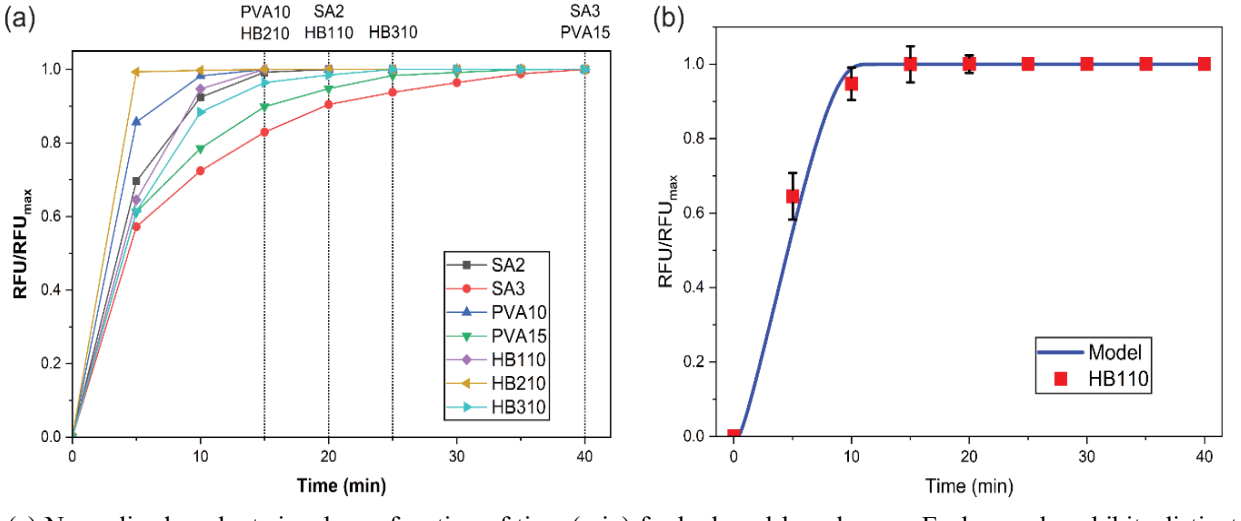

Fig. 8: (a) Normalized readout signal as a function of time (min) for hydrogel-based assay. Each sample exhibits distinct reaction kinetics, with most reaching a maximum readout signal within 40 minutes. Vertical bars show corresponsive maximum readout point of each formulation, and (b) Curve fitting of the computational model with the readout profile of HB110.

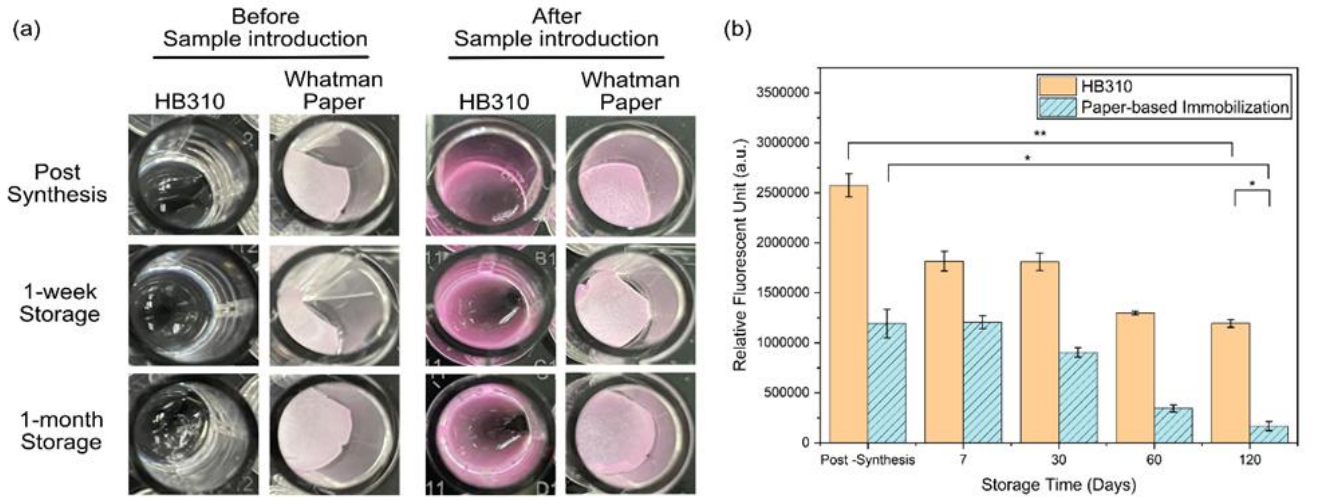

Fig. 9: (a) Visual readout of HB310 and paper-based assays post-synthesis and after storage and (b) Relative fluorescent intensity measured from HB310 and paper-based assays post-synthesis and after storage.

total of 14 runs to construct a quadratic model. Statistical analysis showed a high predictive performance, with an R^2 value of 0.995, and all terms being significant ($p < 0.05$), except for the interaction term between enzyme concentration and hydrogel thickness. From Fig. 10, a higher enzyme concentration resulted in reduced signal readout times, suggesting that the system is reaction-limited at a substrate diffusivity of 4×10^{-12} m/s. Substrate diffusivity within the gel matrix emerged as a critical factor, with higher diffusivity enhancing the speed of substrate-enzyme interaction, thus shortening the signal readout time. Hydrogel thickness in the range of 0.2 – 1 mm showed lesser influence. This could due to the small assay radius, which allows for the rapid saturation of uric acid in the thin gel matrix. This is evident in the observed spike in the uric acid concentration profile simulated by the mathematical model during time t_{drop} (not shown).

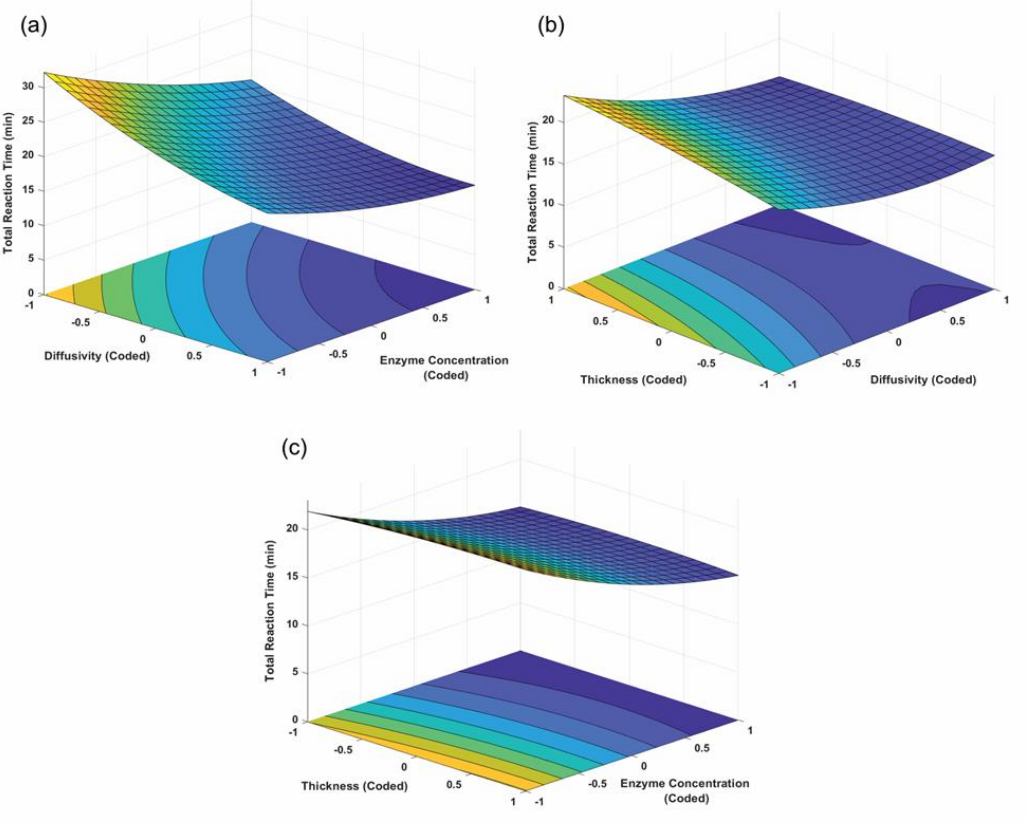

Fig. 10: Surface plots illustrating the influence of different coded parameters on total reaction time (min). (a) Effect of diffusivity and enzyme concentration, (b) effect of thickness and diffusivity, and (c) effect of thickness and enzyme concentration. The color gradients represent variations in reaction time, with contour projections shown on the base of each plot.

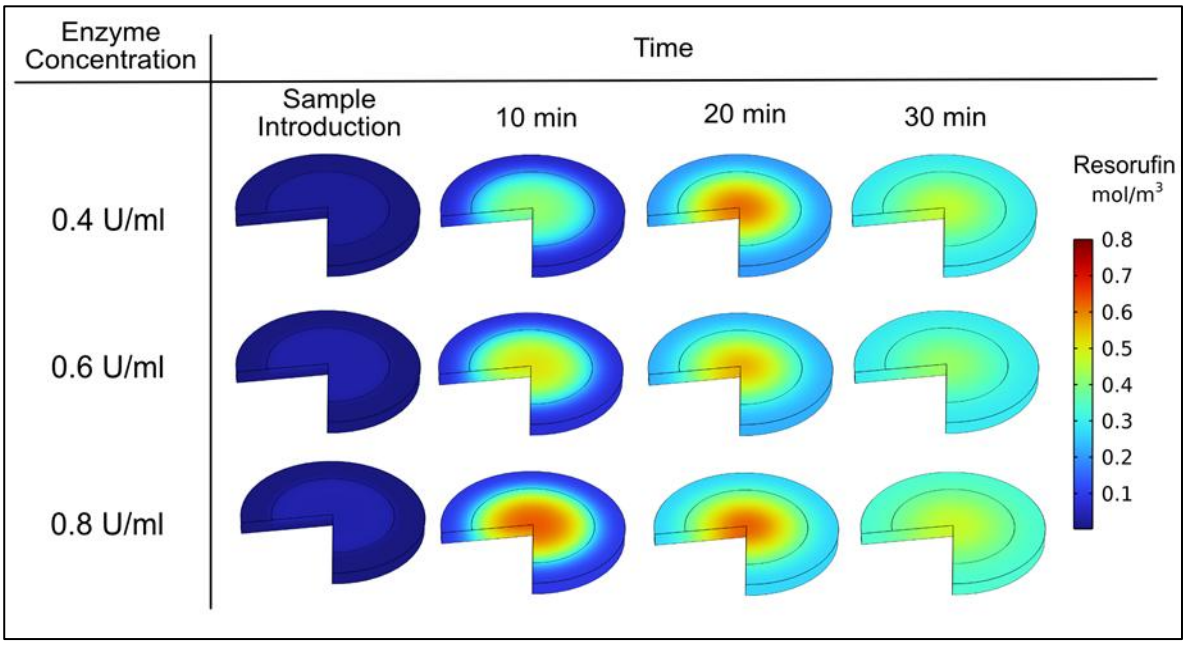

Fig. 11: Surface plots of dynamic resorufin generation simulated through a mathematical model with different enzyme concentrations. The model is simulated with different immobilized uricase units.

Fig. 11 shows the simulated dynamic visual intensity of resorufin at different enzyme concentrations. Visually, the uniformity of fluorescent readout was achieved faster with a higher concentration of immobilized uricase. Interestingly, integration across the hydrogel volume revealed a plateaued rate of resorufin generation at a uricase concentration of 0.8 U/mL, suggesting a shift toward a diffusion-limited system as enzymatic reactions accelerate. This phenomenon is well-illustrated in Fig. 10(a), which shows the interaction effects of enzyme concentration and uric acid diffusivity on the final readout time.

The results demonstrated the promising adaptation of mathematical modeling for hydrogel-based assay development. Nonetheless, relevant parameters, including gel porosity, adsorption kinetic constant, and enzyme inhibition effects, should be studied in future work to ensure the economic viability of the assay.

4. Conclusion

The hydrogel-based assay for rapid uric acid quantification was successfully developed. Hydrogel formulations, including pure alginate, pure PVA, and hybrid hydrogels, were evaluated for their physical properties, swelling behavior, and performance in uric acid detection. Hybrid hydrogels demonstrated the most promising characteristics, including minimal shrinkage, suitable porosity, and optimal swelling behavior, contributing to their superior assay performance. The hydrogel-based assay exhibited a competitive linear range of 2–600 µM with a low limit of detection (LOD) of 1.92 µM, making it effective for preliminary hyperuricemia screening. Additionally, the assay showed prolonged stability, maintaining significant enzyme activity even after 120 days of storage, outperforming conventional paper-based assays. Integrating a mathematical model further validated the experimental results and provided insights into the parametric influences on assay performance. These findings suggest that the hydrogel-based assay could be a viable and cost-effective alternative to existing uric acid detection methods, with potential applications in both clinical and at-home settings. Further studies are recommended to optimize the hydrogel matrix and explore the detection of other analytes using similar methodologies.

Acknowledgements

This research project is supported by Mahidol University (MU's Strategic Research Fund: 2023).

Conflict of Interest

There is no conflict of interest.

Supporting Information

Not applicable.

References

[1] T. Bardin, P. Richette, Definition of hyperuricemia and gouty conditions, *Current Opinion in Rheumatology*, 2014, **26**, 186-191, doi: 10.1097/BOR.0000000000000028.

[2] M. Meller, A. Epstein, A. Y. Meller, F. A. Osmani, A. Parekh, D. Chuang, M. Gonzalez, Hyperuricemia and gout in orthopaedics, *JBJS Reviews*, 2018, **6**, e11, doi: 10.2106/JBJS.RVW.17.00206.

[3] C. E. M. Landa, Renal effects of hyperuricemia, *Contributions to Nephrology*, 2018, **192**, 8-16, doi: 10.1159/000484273.

[4] A. A. Ejaz, R. J. Johnson, M. Shimada, R. Mohandas, K. F. Alquadan, T. M. Beaver, V. Lapsia, B. Dass, The role of uric acid in acute kidney injury, *Nephron*, 2019, **142**, 275-283, doi: 10.1159/000499939.

[5] D. Grassi, L. Ferri, G. Desideri, P. Di Giosia, P. Cheli, R. Del Pinto, G. Properzi, C. Ferri, Chronic hyperuricemia, uric acid deposit and cardiovascular risk, *Current Pharmaceutical Design*, 2013, **19**, 2432-2438, doi: 10.2174/1381612811319130011.

[6] J. C. Ramirez-Sandoval, M. Madero, Treatment of hyperuricemia in chronic kidney disease, *Uric Acid in Chronic Kidney Disease*, 2018, **192**, 135-146, doi: 10.1159/000484288.

[7] J. T. Kielstein, R. Pontremoli, M. Burnier, Management of hyperuricemia in patients with chronic kidney disease: a focus on renal protection, *Current Hypertension Reports*, 2020, **22**, 102, doi: 10.1007/s11906-020-01116-3.

[8] M. Skoczyńska, M. Chowaniec, A. Szymczak, A. Langner-Hetmańczuk, B. Maciążek-Chyra, P. Wiland, Pathophysiology of hyperuricemia and its clinical significance - a narrative review, *Reumatologia*, 2020, **58**, 312-323, doi: 10.5114/reum.2020.100140.

[9] V. Lohsoonthorn, B. Dhanamun, M. A. Williams, Prevalence of hyperuricemia and its relationship with metabolic syndrome in Thai adults receiving annual health exams, *Archives of Medical Research*, 2006, **37**, 883-889, doi: 10.1016/j.arcmed.2006.03.008.

[10] Y. Zhang, H. Yu, S. Chai, X. Chai, L. Wang, W. Geng, J. Li, Y. Yue, D. Guo, Y. Wang, Noninvasive and individual-centered monitoring of uric acid for precaution of hyperuricemia via optical supramolecular sensing, *Advanced Science*, 2024, **9**, 2104463, doi: 10.1002/advs.202104463.

[11] L. Liao, C. Liao, C. Liu, T. Yang, G. Wang, Evaluation of an electrochemical biosensor for uric acid measurement in human whole blood samples, *Clinica Chimica Acta*, 2014, **436**, 72-77, doi: 10.1016/j.cca.2014.04.033.

[12] K. M. Koczula, A. Gallotta, Lateral flow assays, *Essays in Biochemistry*, 2016, **60**, 111-120, doi: 10.1042/ebc20150012.

[13] D. Gasperino, T. Baughman, H. V. Hsieh, D. Bell, B. H. Weigl, Improving lateral flow assay performance using computational modeling, *Annual Review of Analytical Chemistry*, 2018, **11**, 219-244, doi: 10.1146/annurev-anchem-061417-125737.

[14] A. Belluati, I. Craciun, J. Liu, C. G. Palivan, Nanoscale enzymatic compartments in tandem support cascade reactions *in vitro*, *Biomacromolecules*, 2018, **19**, 4023-4033, doi: 10.1021/acs.biomac.8b01019.

[15] Y. Zhou, M. Zhang, D. He, X. Hu, H. Xiong, J. Wu, B. Zhu, J. Zhang, Uricase alkaline enzymosomes with enhanced stabilities and anti-hyperuricemia effects induced by favorable microenvironmental changes, *Scientific Reports*, 2016, **7**, 20136, doi: 10.1038/srep20136.

[16] C. Geraths, M. Daoud-El Baba, G. Charpin-El Hamri, W. Weber, A biohybrid hydrogel for the urate-responsive release of urate oxidase, *Journal of Controlled Release*, 2013, **171**, 57-62, doi: 10.1016/j.jconrel.2013.06.037.

[17] T. R. Hoare, D. S. Kohane, Hydrogels in drug delivery: Progress and challenges, *Polymer*, 2008, **49**, 1993-2007, doi: 10.1016/j.polymer.2008.01.027.

[18] M. S. Gil, J. Cho, T. Thambi, V. H. Giang Phan, I. Kwon, D. S. Lee, Bioengineered robust hybrid hydrogels enrich the stability and efficacy of biological drugs, *Journal of Controlled Release*, 2017, **267**, 119-132, doi: 10.1016/j.jconrel.2017.04.009.

[19] T. Yoshii, S. Onogi, H. Shigemitsu, I. Hamachi, Chemically reactive supramolecular hydrogel coupled with a signal amplification system for enhanced analyte sensitivity, *Journal of the American Chemical Society*, 2015, **137**, 3360-3365, doi: 10.1021/ja5131534.

[20] T. Falohun, M. J. McShane, An optical urate biosensor based on urate oxidase and long-lifetime metalloporphyrins, *Sensors*, 2020, **20**, 959, doi: 10.3390/s20040959.

[21] P. Rastogi, B. Kandasubramanian, Review of alginate-based hydrogel bioprinting for application in tissue engineering, *Biofabrication*, 2019, **11**, 042001, doi: 10.1088/1758-5090/ab331e.

[22] J. Li, H. Wei, S. Cui, H. Hou, Y. Zhang, Y. Zhang, B. X. Ben, L. Chu, Z. M. El-Bahy, S. Melhi, R. Sellami, Z. Guo, Polyvinyl alcohol/sodium alginate-based conductive hydrogels with *in situ* formed bimetallic zeolitic imidazolate frameworks towards soft electronics, *Carbohydrate Polymers*, 2024, **346**, 122633, doi: 10.1016/j.carbpol.2024.122633.

[23] Z. Wu, X. Liu, Q. Xu, L. Zhang, S. N. Abdou, M. M. Ibrahim, J. Zhang, Z. M. El-Bahy, N. Guo, J. Gao, L. Weng, Z. Guo, Poly(vinyl alcohol)/polyacrylamide double-network ionic conductive hydrogel strain sensor with high sensitivity and high elongation at break, *Journal of Polymer Science*, 2024, **62**, 4599-4611, doi: 10.1002/pol.20240209.

[24] L. Fu, A. Yu, G. Lai, Conductive hydrogel-based electrochemical sensor: a soft platform for capturing analyte, *Chemosensors*, 2021, **9**, 282, doi: 10.3390/chemosensors9100282.

[25] J. Tavakoli, Y. Tang, Hydrogel based sensors for biomedical applications: an updated review, *Polymers*, 2017, **9**, 364, doi: 10.3390/polym9080364.

[26] A. Sonawane, P. Manickam, S. Bhansali, Stability of enzymatic biosensors for wearable applications, *IEEE Reviews in Biomedical Engineering*, 2017, **10**, 174-186, doi:

10.1109/RBME.2017.2706661.
[27] J. Lu, Y. Xiong, C. Liao, F. Ye, Colorimetric detection of uric acid in human urine and serum based on peroxidase mimetic activity of MIL-53(Fe), *Analytical Methods*, 2015, **7**, 9894-9899, doi: 10.1039/C5AY02240A.
[28] F. Li, T. He, S. Wu, Z. Peng, P. Qiu, X. Tang, Visual and colorimetric detection of uric acid in human serum and urine using chitosan stabilized gold nanoparticles, *Microchemical Journal*, 2021, **164**, 105987, doi: 10.1016/j.microc.2021.105987.
[29] U. Nishan, W. Ullah, N. Muhammad, M. Asad, S. Afridi, M. Khan, M. Shah, N. Khan, A. Rahim, Development of a nonenzymatic colorimetric sensor for the detection of uric acid based on ionic liquid-mediated nickel nanostructures, *ACS Omega*, 2022, **7**, 26983-26991, doi: 10.1021/acsomega.2c04070.
[30] X. Wang, Q. Yao, X. Tang, H. Zhong, P. Qiu, X. Wang, A highly selective and sensitive colorimetric detection of uric acid in human serum based on MoS_2-catalyzed oxidation TMB, *Analytical and Bioanalytical Chemistry*, 2019, **411**, 943-952, doi: 10.1007/s00216-018-1524-6.
[31] C. Liang, Y. Lan, Z. Sun, L. Zhou, Y. Li, X. Liang, X. Qin, Synthesis of carbon quantum dots with iron and nitrogen from Passiflora edulis and their peroxidase-mimicking activity for colorimetric determination of uric acid, *Mikrochimica Acta*, 2020, **187**, 405, doi: 10.1007/s00604-020-04391-8.
[32] J. Pantakitcharoenkul, J. Touma, G. Jovanovic, M. Coblyn, Enzyme-functionalized hydrogel film for extracorporeal uric acid reduction, *Journal of Biomedical Materials Research Part B: Applied Biomaterials*, 2024, **112**, e35375, doi: 10.1002/jbm.b.35375.